THE FRACTURE TOUGHNESS - MICROSTRUCTURE RELATIONSHIP OF ALUMINA-BASED CERAMICS

B.J. Dalgleish, A. Fakhr, P.L. Pratt and R.D. Rawlings

Department of Metallurgy and Materials Science, Imperial College, London, SW7 2BP, England.

ABSTRACT

Samples of commercial sintered alumina, and alumina-zirconia composites have been characterised in terms of grain size and porosity, and the presence of second phase inclusions. Measurements of the fracture toughness and acoustic response of the materials have been made using the SENB test, and the results have been interpreted in terms of observed microstructure.

KEYWORDS

Alumina, alumina-zirconia composites, fracture toughness, acoustic emission, transformation toughening.

INTRODUCTION

The technique of acoustic emission has been employed in the mechanical testing of ceramics (Evans and Linzer, 1973; Evans, Linzer and Russell, 1974; Evans and Graham, 1975; Schuldies, 1973), to monitor the elastic stress waves released as a result of sudden changes in elastic strain energy due to dynamic processes such as crack propagation. In particular, the work of the present authors (Dalgleish et al 1979, 1980) has demonstrated that acoustic emission may be used successfully to detect subcritical crack growth during the fracture toughness testing of aluminas over the temperature range 20-1000°C. The earlier work was carried out on isostatically cold-pressed and fired aluminas and this paper reports the results of an extension of the research programme to hot-pressed alumina, and hot-pressed alumina containing particles of unstabilised ZrO_2.

EXPERIMENTAL PROCEDURE

Materials

Three aluminas were investigated; two had been isostatically cold-pressed and fired on commercial schedules (designated FAO^x and A^+), and the third had been hot-pressed from Alcoa A-16 powder (H^*).

x supplied by Smith Industries Ltd. + by Anderman and Ryder Ltd. *by N. Claussen.

The purities quoted by the manufacturers were 95, 97.5 and 99.7% for FAO, A and H respectively. Three $Al_2O_3.ZrO_2$ samples* containing 12, 15 and 18 $^{V}/_{o}$ ZrO_2 of average particle size 2μm were also investigated. These were hot-pressed from Alcoa A-16 alumina and unstablised ZrO_2 powder as described previously (Claussen, 1976; Claussen, Steeb and Pabst, 1977). Reflected light microscopy was used to characterise the microstructures of the aluminas, and bulk densities were calculated from mass volume measurements of carefully machined plates.

Mechanical Testing

Single edge-notched bend (SENB) specimens with dimensions typically 25 x 4 x 2 mm and $a_o/w = 0.5$ were prepared from the aluminas and the $Al_2O_3.ZrO_2$ composites. The initial crack, of length a_o, was cut using a 0.25 mm thick, diamond impregnated, annular saw, and the specimens were tested at room temperature on a screw-driven Instron machine at a cross head speed of 0.1 mm/min. The critical stress intensity factor was determined from the expression:

$$K_{IC} = \frac{3P_F S Y a_o^{\frac{1}{2}}}{2bw^2} \qquad 1$$

where P_F = fracture load, S = loading span and Y = calibration factor to account for allowed variations in the a_o/w ratio.

Specimens of the three aluminas, typically 25 x 3 x 3 mm in size, were tested in 3-point bending at a crosshead speed of 0.1 mm/min. The modulus of rupture (MOR) σ_f, was calculated using the equation

$$\sigma_f = \frac{3P_F S}{2bw^2} \qquad 2$$

The fracture surfaces were subsequently examined in the scanning electron microscope, the specimens being coated with a 200Å layer of gold to prevent charging.

Acoustic Emission

The acoustic response during mechanical testing was detected using a miniature PZT resonant transducer, which was coupled to the specimens with grease and held in position with a spring clip. The output of the transducer was amplified and monitored with standard Dunegan-Endevco acoustic emission equipment capable of ring-down and event counting together with facilities for measuring amplitude distributions. The amplitude distributions were analysed using a power law (Pollock 1973) namely:

$$n(a) = (a/a_o)^{-b} \qquad 3$$

where n(a) is the fraction of the emission population whose peak amplitude exceeds a, a_o is the lowest detectable amplitude, and the exponent b characterises the amplitude distribution.

RESULTS

Materials Characterisation

The density, porosity and grain size characteristics of the aluminas and $Al_2O_3.ZrO_2$ composites are presented in Table I, and the differences in grain size and porosity of the aluminas are illustrated in the optical micrographs of Figure 1.

TABLE I. The Microstructural Characteristics of the Materials.

Material	Density ($x10^3 Kgm^{-3}$)	Porosity %	Grain Size (μm) Mean	Max.	Maximum Pore size (μm)	Purity %
FAO	3.75	6.0	4	35	30	95
A	3.79	4.3	3	15	14	97.5
H	3.92	1.7	1.2	5	3	99.7
12%ZrO_2	4.17	1.7	1.2	6	3	-
15%ZrO_2	4.22	1.9	1.2	5	3	-
18%ZrO_2	4.28	2.1	1.2	6	3	-

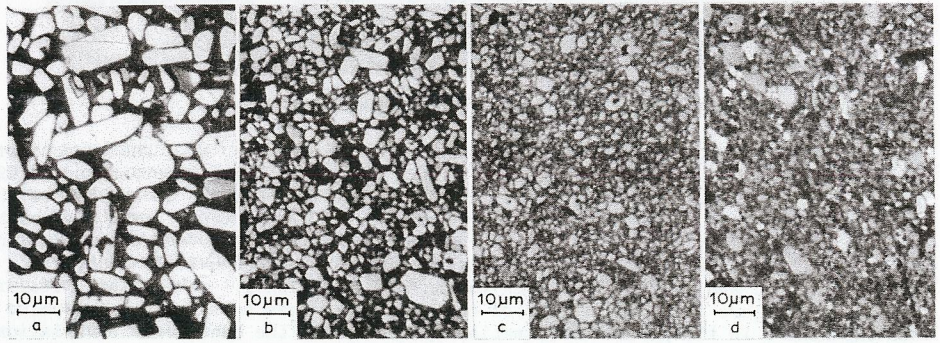

Fig. 1. Optical micrographs of (a) FAO (b) A (c) H and (d) $Al_2O_3ZrO_2$.

The microstructure of FAO consisted of a matrix of fine-grained material which contained a significant number of large grains, some approaching 35μm in diameter. The porosity was mainly intergranular, rounded, and generally smaller than the coarse grains.

Alumina A contained grains up to 15μm in diameter within a fine grained matrix. The porosity generally consisted of isolated, angular, intergranular voids, although in some regions the pores were interconnected. Most of the pores were less than 5μm.

The hot pressed alumina H displayed the finest grain structure and the lowest percentage porosity of the three aluminas. Furthermore, there was little variation in the grain and pore sizes compared with the broad distributions found in aluminas FAO and A. The maximum pore size was 3μm, the porosity being a mixture of rounded intra-and intergranular pores, and some angular intergranular pores.

The microstructure of the two-phase $Al_2O_3ZrO_2$ was very similar to that of the hot pressed alumina H except for the presence of small ZrO_2 particles of mean diameter 2μm (Figure 1d), and some associated microcracking (Figure 2). X-ray mapping using energy dispersive analysis confirmed that the lighter coloured grains were ZrO_2. Occasionally ∿30μm regions of poorly sintered ZrO_2 were observed, but extensive examination showed that they were not a general feature of the structure and thus would be unlikely significantly to affect the mechanical properties.

Mechanical Properties and Acoustic Emission

For all the SENB specimens the acoustic emission commenced at a load, P_S, which was

less than the fracture load, P_F, even though there was a linear relationship between load and displacement up to P_F. It has been shown previously (Dalgleish et al, 1979; Dalgleish et al, 1980) that the emissions prior to failure in a fracture toughness test are associated with subcritical crack growth.

Fig. 2. SEM of Al_2O_3.18%ZrO_2 showing linked radial microcracks.

The average number of ring-down counts, N_{RT}, and event counts, N_{ET}, due to activity prior to final failure, were quantified by measuring the counts occurring up to 99% of the fracture load P_F. In general, this accounted for between 50 and 80% of the total ring-down and event counts monitored at the end of the test. The N_{RT} and N_{ET} results for aluminas FAO, A and H are presented along with other acoustic emission data, in Table II, which also includes as-measured K_{IC} values calculated by insertion of P_F and the initial crack length into equation 1. The notable features of the results are the small number of counts for aluminas A and H, the low value of the exponent b in the power law (equation 3) for H, and the considerable variation in the value of K_{IC} for the three aluminas. The amplitude distributions showed that the difference in N_{ET} and the b-value are due to an increasing number of low energy events in the sequence H<A<FAO. The smaller the number of acoustic events detected prior to failure the lower was the final b-value (Table II), which indicates that the events associated with subcritical crack growth are mainly of low energy.

TABLE II. The Fracture Toughness and Acoustic Response of the Aluminas.

Alumina	N_{RT} x 10^2	N_{ET}	b	P_S/P_F	K_{IC} ($MNm^{-3/2}$) As measured	Corrected via N_{ET}	Corrected via PS/PF
FAO	140±84	100±32	1.02	0.96	4.85±0.2	4.99	5.00
A	27±8	33±15	0.94	0.94	3.82±0.31	3.88	4.00
H	15±6	30±16	0.74	0.98	6.09±0.67	-	6.18

The presence of ZrO_2 particles significantly altered the fracture toughness and the acoustic emission as shown in Figure 3. The dependence of all the parameters measured, i.e. K_{IC}, b, N_{ET} and N_{RT}, on the volume percentage of ZrO_2 was similar, with the maxima occurring at 12%ZrO_2. The amplitude distributions for the Al_2O_3.ZrO_2 samples (Figure 4) show that the event increment associated with the ZrO_2 particles is mainly due to an increase in the number of low energy events.

The load-displacement curves in the modulus of rupture tests were linear up to the fracture stress, σ_F, but no acoustic emission was detected prior to the onset of catastrophic failure. The b-value and the total number of ring-down and event counts were less than those monitored during the SENB tests (Table III).

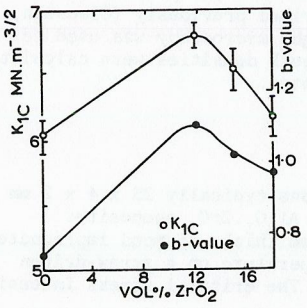

Fig. 3. K_{IC}, b and ZrO_2 content.

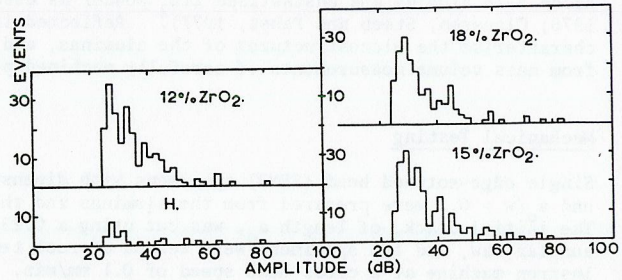

Fig. 4. Amplitude distribution and ZrO_2 content.

The different acoustic emission characteristics observed in the two types of mechanical test were accounted for by the larger number of low energy emissions in the SENB tests. Nevertheless, the MOR results showed the same trend as the SENB results, namely the number of events increased in the sequence H<A<FAO. Comparison of the mechanical property data of Table II and III shows that alumina H exhibited the highest values of K_{IC} and σ_F. The K_{IC} value for FAO was greater than that for A, but the trend was reversed for the σ_F values.

TABLE III. Modulus of Rupture (σ_F) and Acoustic Response of the Aluminas.

Alumina	N_{RT}	N_{ET}	b	σ_F ($MN.m^{-2}$)
FAO	2800±400	45±17	0.68	340±20
A	980±185	25±9	0.60	414±14
H	280±94	11±4	0.55	550±26

When examined at low magnification the fracture surfaces of the Al_2O_3.ZrO_2 specimens appeared more undulating compared with those of aluminas H (Figure 5a) and A, and the coarse, but overall planar, surface of FAO. Additional features apparent at low magnification were the presence of side-branching, particularly in the 15 and 18%ZrO_2 specimens (Figure 5b), and the susceptibility of alumina A to pull-out. The fracture mode of each of the materials was predominately intercrystalline, although transcrystalline failure of the occasional large grain was observed. In the case of the ZrO_2-containing aluminas many ZrO_2 particles were found on the fracture surface, isolated and almost detached from the surrounding Al_2O_3 (Figure 5c).

DISCUSSION

Aluminas FAO, A and H

The acoustic emission prior to failure in the SENB tests was the result of subcritical crack growth. To obtain accurate K_{IC} values the crack length substituted into equation (1) should be corrected to account for the growth of the initial crack.

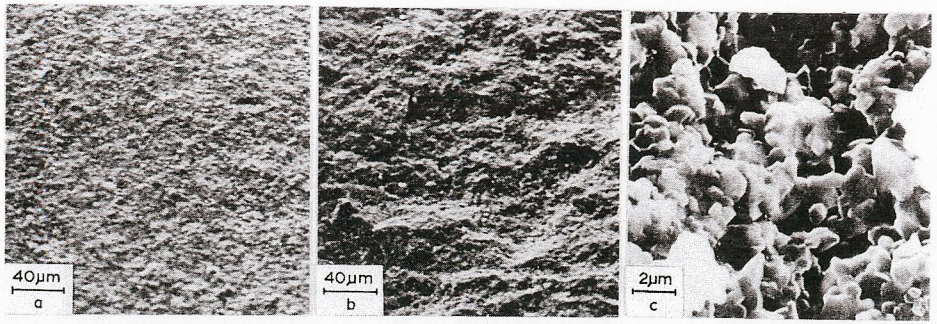

Fig. 5. Scanning Electron Fractographs of (a) H, (b) and (c) $Al_2O_3$18%ZrO_2 Samples.

The extent of sub-critical crack growth was determined from experimentally obtained correction curves (Dalgleish et al 1980) and from the empirical relationship:

$$\frac{a_o}{a_F} = \tfrac{1}{2}(1 + P_S/P_F)$$

where a_o and a_F are the initial and final crack lengths. The corrected values for K_{IC} are given in Table II and it can be seen that for the test conditions employed the corrections are small for the three aluminas.

The high K_{IC} for alumina H was a consequence of the small grain size and the low percentage of porosity, much of which was rounded, whereas the poor fracture toughness of A was due to the relatively large amount of angular porosity. The rounded nature of the porosity in FAO outweighed the large grain size and high porosity content to yield an intermediate value for K_{IC}.

The acoustic response prior to failure depends on the extent of sub-critical crack growth, and the number of counts per unit area of sub-critical crack extension. For alumina the latter is predominantly dependent on purity, whilst the extent of sub-critical crack growth is also affected by grain size and porosity. As a general guide, the more acoustic emission counts that are monitored prior to failure the greater the grain size, the greater the porosity content and the more impure the alumina. However, this generalisation does not always hold when comparing the acoustic emission from a series of very similar materials, as is apparent from the $Al_2O_3.ZrO_2$ data.

The modulus of rupture σ_F is a function of the ease of critical flaw nucleation and propagation, the latter being quantified by K_{IC}. The low σ_F value for FAO is attributed to the large initial flaws, as specified by the maximum pore and grain areas, compared with those of aluminas A and H (Table IV). The small initial flaw size and the high K_{IC} accounts for the good modulus of rupture value of H.

The critical flaws in alumina are often semi-elliptical surface flaws (Meredith and Pratt, 1975) and for such a flaw it has been shown that:

$$\sigma_F = 1.68\ K_{IC}/YA^{\frac{1}{4}}$$

where A is the critical flaw area. The calculated critical flaw areas are considerably larger than the initial flaw sizes (Table IV), therefore flaw linking must have occurred prior to major crack propagation.

TABLE IV. Flaw Sizes and Estimated Acoustic Emission.

Alumina	Maximum Initial Flaw Area $(\mu m)^2$		Flaw Area (Calculated) $A(\mu m^2)$	Estimated AE	
	Pore	Grain		N_{RT}	N_{ET}
FAO	7.1×10^2	96×10^2	315×10^2	3050	50
A	1.5×10^2	1.8×10^2	55×10^2	190	7
H	7	20	115×10^2		

The correction curves may be used to estimate the number of acoustic emission counts associated with the production of a critical flaw if it is assumed that the mechanism of linkage of the initial flaws to critical size takes place by a similar mechanism to sub-critical crack growth in SENB tests. The maximum number of counts estimated are given in Table IV, the area of the initial flaws being ignored. The estimated number of counts is not insignificant when compared with the monitored counts (Table III) and would have been detected, if emitted prior to failure, and if they were of similar energy to the emissions accompanying sub-critical crack growth in SENB tests. As no acoustic emission was detected prior to failure in the MOR tests it is concluded that the unit step in the linkage process is smaller than that in sub-critical crack growth along an extended crack front in an SENB test. Consequently the acoustic emission due to linkage is of even lower energy than that associated with sub-critical crack growth and is below the noise level of the equipment. The amplitude distributions and b-values from the SENB and MOR tests are consistent with this suggestion in that the SENB distributions have a large number of low energy events, associated with sub-critical crack growth, and high b-values (0.74 to 1.02). As linkage emission is not detected in the MOR tests, the distributions correspond solely to events accompanying final failure and are characterised by low b-values (0.55 to 0.68).

$Al_2O_3.ZrO_2$ Composites

In this section K_{IC} refers to the as-measured value, as the correction for sub-critical crack growth is small and does not alter the dependence on ZrO_2 content. The change in toughness with volume percentage ZrO_2 (Figure 3) was similar to that reported by Claussen,1976 and Claussen, Steeb and Pabst, 1977, who interpreted the data in terms of micro-cracking of the matrix resulting from the expansion accompanying the tetragonal to monoclinic transformation of the ZrO_2 particles. The energy absorbed in opening up micro-cracks in a zone immediately in front of the main crack, and by crack branching was considered to be responsible for the improved fracture resistance of the two-phase materials.

In the present investigation the fracture surfaces of the $Al_2O_3.ZrO_2$ specimens were undulating, consistent with crack branching, and microstructural examination confirmed the presence of micro-cracking associated with ZrO_2 particles. Generally the cracking was in the Al_2O_3, radial from the particles (Figure 2), but sometimes cracking was evident at the ZrO_2/Al_2O_3 interface and within the ZrO_2 particles. At low ZrO_2 contents the micro-cracking was isolated, being associated with individual ZrO_2 particles, but at high volume percentages (15 and 18%) the radial cracks were often linked as shown in Figure 2. Claussen has suggested that the linking of the micro-cracks leads to the observed fall in K_{IC} at high volume percentages of ZrO_2.

All the $Al_2O_3.ZrO_2$ samples were acoustically noisier than the hot-pressed alumina and, as shown in Figure 4, most of the extra acoustic events were of low energy. This is in agreement with the proposed microcrack model, since the opening of micro-cracks would occur frequently and would be a low energy process. As the volume percentage of ZrO_2 increased, leading to micro-crack linkage, so the number of isolated micro-cracks opening decreased, giving fewer low energy events and reduced b-values (Figures 3 and 4).

CONCLUSIONS

i) Good mechanical properties are encouraged in a single-phase alumina by small grain size, high density, and rounded pores. In general, the acoustic emission associated with subcritical crack growth in an SENB test is more marked the greater the grain size, the greater the percentage porosity, and the more impure the alumina. Acoustic emission resulting from the production of the critical flaw in an MOR test is not detected.

ii) The mechanical properties of alumina are improved by the addition of an optimum volume percentage of dispersed fine ZrO_2 particles. This improvement is believed to be due to the opening of micro-cracks, and the present microscopy results and acoustic emission data are consistent with this explanation. Excessive additions of ZrO_2 lead to micro-crack linkage and a consequent deterioration of mechanical properties.

REFERENCES

Claussen, N. (1976). Fracture toughness of Al_2O_3 with an unstabilised ZrO_2 dispersed phase. J. Am. Ceram. Soc., 59, 49-51.

Claussen, N., J. Steeb and R.F. Pabst (1977). Effect of induced microcracking on the fracture toughness of ceramics. Ceramic Bulletin, 56, 559-562.

Dalgleish, B.J., A. Fakhr, P.L. Pratt and R.D. Rawlings (1979). The temperature dependence of the fracture toughness and acoustic emission of polycrystalline alumina. J. Mat. Sci., 14, 2605-2615.

Dalgleish, B.J., A. Fakhr, P.L. Pratt and R.D. Rawlings (1980). Fracture toughness testing of ceramics and acoustic emission. Accepted for publication in Mat. Sci. and Eng.

Evans, A.G. and M. Linzer (1973). Failure prediction in structural ceramics using acoustic emission. J. Am. Ceram. Soc., 56, 575-579.

Evans, A.G., M. Linzer and L.R. Russell (1974). Acoustic emission and crack propagation in polycrystalline alumina. Mat.Sci. and Eng., 15, 253-261.

Evans, A.G., and L.J. Graham (1975). A model for crack propagation in polycrystalline ceramics. Acta Met., 23, 1303-1312.

Meredith, H. and P.L. Pratt (1975). The observed fracture stress and measured values of K_{IC} in commercial polycrystalline aluminas. In P. Popper (Ed.) Special Ceramics, 6, The British Ceramic Research Association, pp.107-122.

Pollock, A.A. (1973). Acoustic emission amplitudes. Acoustic Emission, 2, Non-Destructive Testing, 6, 223.

Schuldies, J.J. (1973). The acoustic emission response of mechanically stressed ceramics. Materials Evaluation, 31, 209.